REPORT

A bio-feedback-mimicking electrode combining real-time monitoring and drug delivery

Shuaiyin Liu,[1] Tianqin Ning,[1] Junlin Chen,[1] Yanzhe Fu,[1] Jiebo Li,[1] Jinyu Li,[2,*] Xufeng Niu,[1,*] and Yubo Fan[1,3,*]

*Correspondence: leery_5566@163.com (J.L.); nxf@buaa.edu.cn (X.N.); yubofan@buaa.edu.cn (Y.F.)

Received: December 14, 2023; Accepted: September 26, 2024; Published Online: September 30, 2024; https://doi.org/10.1016/j.xinn.2024.100705

GRAPHICAL ABSTRACT

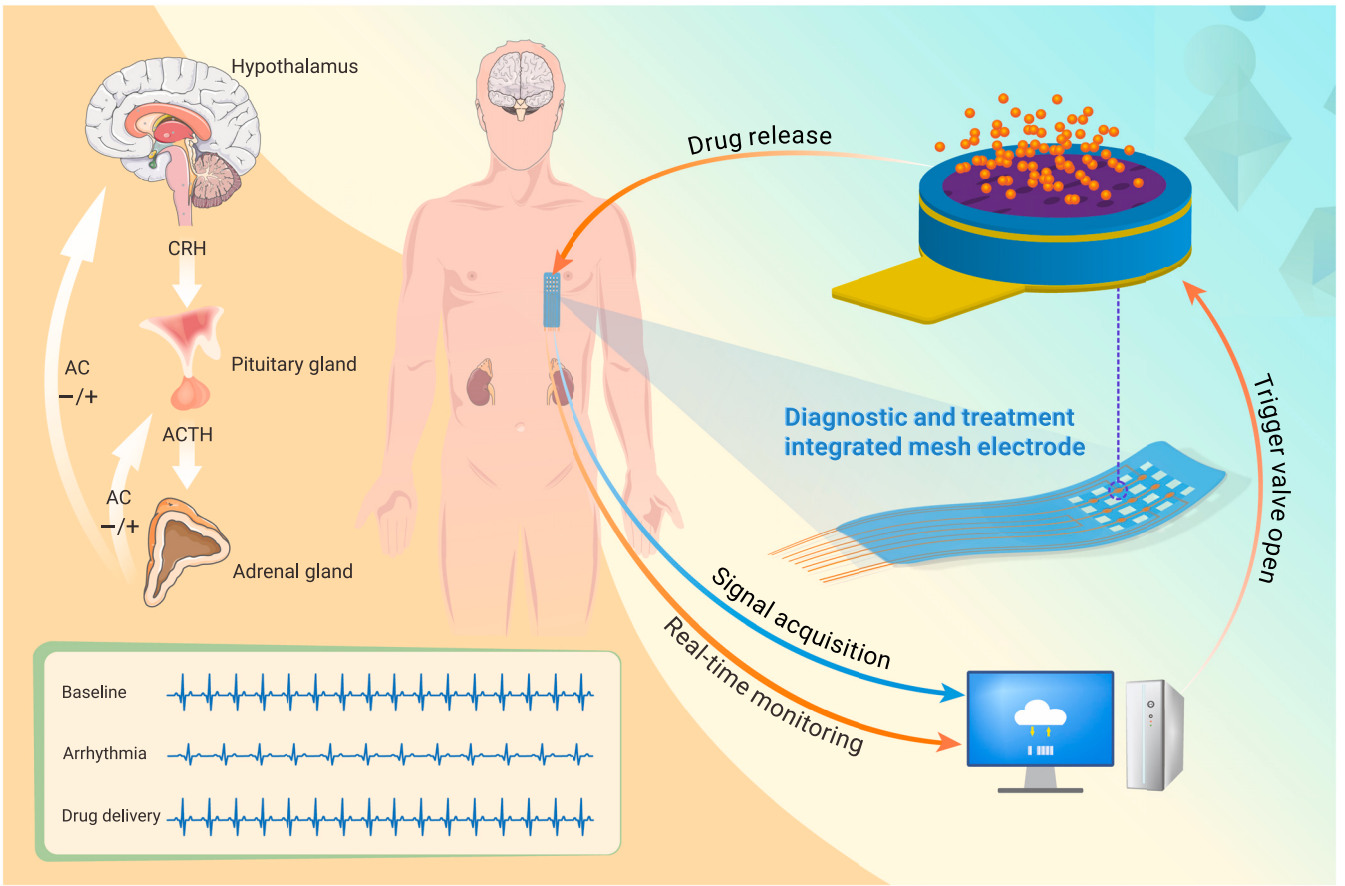

PUBLIC SUMMARY

- This study presents a novel flexible electrode system that integrates drug administration with real-time monitoring.
- Real-time electrophysiological acquisition following drug delivery enables timely and informed disease management.
- This approach enhances medical efficiency while reducing the demand for medical resources.

REPORT

A bio-feedback-mimicking electrode combining real-time monitoring and drug delivery

Shuaiyin Liu,[1] Tianqin Ning,[1] Junlin Chen,[1] Yanzhe Fu,[1] Jiebo Li,[1] Jinyu Li,[2,*] Xufeng Niu,[1,*] and Yubo Fan[1,3,*]

[1]Key Laboratory of Biomechanics and Mechanobiology (Beihang University), Ministry of Education, Beijing Advanced Innovation Center for Biomedical Engineering, School of Biological Science and Medical Engineering, Beihang University, Beijing 100083, China

[2]Department of Orthopedic, Dongzhimen Hospital, Beijing University of Chinese Medicine, Beijing 100007, China

[3]School of Engineering Medicine, Beihang University, Beijing 100083, China

*Correspondence: leery_5566@163.com (J.L.); nxf@buaa.edu.cn (X.N.); yubofan@buaa.edu.cn (Y.F.)

Received: December 14, 2023; Accepted: September 26, 2024; Published Online: September 30, 2024; https://doi.org/10.1016/j.xinn.2024.100705

Citation: Liu S., Ning T., Chen J., et al., (2024). A bio-feedback-mimicking electrode combining real-time monitoring and drug delivery. The Innovation **5(6)**, 100705.

Effective disease management based on real-time physiological changes presents a significant clinical challenge. A flexible electrode system integrating diagnosis and treatment can overcome the uncertainties associated with treatment progress during localized interventions. In this study, we develop a system featuring a biomimetic feedback regulation mechanism for drug delivery and real-time monitoring. To prevent drug leakage, the system incorporates a magnesium (Mg) valve in the outer layer, ensuring zero leakage when drug release is not required. The middle layer contains a drug-laden poly(3,4-ethylenedioxythiophene) (PEDOT) sponge (P-sponge), which supplies the water to partially or fully activate the Mg valve under electrical stimulation and initiate drug release. Once the valve is fully opened, the exposed and expanded P-sponge electrode establishes excellent contact with various tissues, facilitating the collection of electrophysiological signals. Encapsulation with polylactic acid film ensures the system's flexibility and bioresorbability, thereby minimizing potential side effects on surrounding tissues. Animal experiments demonstrate the system's capability to mimic feedback modulation mechanisms, enabling real-time monitoring and timely drug administration. This integrated diagnosis and treatment system offers an effective solution for the emergency management of acute diseases in clinical settings.

INTRODUCTION

Effective clinical disease management hinges on the accurate diagnosis and timely treatment of conditions. Traditionally, these two modalities have been approached separately, leading to inefficiencies, delayed responses, and a lack of real-time monitoring during the course of treatment.[1,2] This separation is particularly problematic in the management of acute diseases, where the disjointed approach can result in missed opportunities for timely intervention, potentially leading to suboptimal outcomes or even fatalities. Additionally, the conventional healthcare system is increasingly strained by the dual pressures of an aging population and the heightened demands posed by epidemics.[3-9] In this context, the development and implementation of wearable diagnostic and therapeutic integrated (DTI) devices, which combine real-time diagnosis with immediate drug delivery, emerge as a promising solution. These devices not only address acute clinical needs more effectively but also help to alleviate the growing burden on healthcare resources.[10,11]

Implantable flexible electrodes have demonstrated significant potential in enabling *in vivo* monitoring of various physiological signals, such as blood pressure,[12,13] electromyogram (EMG),[14,15] electrocardiogram (ECG),[13-17] electrocorticogram (ECoG), and electroencephalogram (EEG),[16,18-21] among others.[22-25] These electrodes have also shown promise in therapeutic applications.[26-31] Recent advancements have led to the development of DTI devices based on these implantable electrodes. By incorporating microfluidic drug delivery channels alongside flexible electrodes into a unified system, researchers have achieved integrated diagnostic and treatment capabilities that have proven beneficial in nerve repair and motor function restoration.[32] The combination of drug delivery and signal acquisition within an array of electrodes has enabled real-time monitoring of cardiomyocyte signals and the adjustment of their activity.[33] Moreover, significant strides have been made in DTI bandages and DTI excipients.[34-37] Despite these advancements, most current DTI devices have limitations. The separation of drug-carrying sites from electrode sites in existing designs often leads to inaccurate diagnostic outcomes, necessitating additional electrode sites to support multifunctionality, which, in turn, increases the overall system size.[35,38,39] Moreover, drug-loaded electrodes made from polymers or hydrogels frequently encounter issues with drug leakage, which hampers precise drug delivery.[33,40,41] Additionally, many integrated electrodes are constructed from non-biodegradable materials, necessitating secondary surgical removal to prevent biotoxicity and foreign body reactions associated with long-term implantation. This requirement for secondary surgery can result in further harm to patients and limits the long-term applicability of these devices *in vivo*.[42-44] Therefore, the ideal DTI device should fulfill several key criteria: (1) it should ensure that diagnosis and treatment sites are overlapped to guarantee consistency between monitoring and treatment locations, (2) it must allow for controlled drug release, and (3) it should be biodegradable, thereby eliminating the need for secondary surgical removal and reducing the risk of additional surgical complications.

In the hypothalamic-pituitary-adrenal axis (HPA axis), the hypothalamus, pituitary gland, and adrenal glands work together to diagnose and respond to stress by sequentially secreting corticotropin-releasing hormone (CRH), adrenocorticotropic hormone (ACTH), and cortisol (Figure 1A).[45] Inspired by this natural feedback mechanism, we developed a diagnostic and treatment integrated mesh electrode (DTME) that mimics the functions of the HPA axis. The DTME system is constructed using a poly(3,4-ethylenedioxythiophene) (PEDOT) sponge (P-sponge), polylactic acid (PLA) film, and a magnesium (Mg) valve, combining both therapeutic and diagnostic capabilities within a single platform. In the DTME system, the pre-opened channel can be used for electrophysiological signal acquisition and monitoring, and based on the analysis of the results, the activation of drug-carrying channels can be triggered for drug delivery. The continuous acquisition and analysis of electrophysiological signals and the multiple controlled release of the drug show the biomimicry of a biofeedback system. Our results demonstrated that the system could accurately collect electrophysiological signals and control drug release, enabling effective management of sudden medical conditions. Although the system's valve only allows for an initial, slight opening, its complete activation still relies on the subsequent supply of more water. However, this gradual activation method reduces the stringent conditions typically required for traditional metal valves to open, thereby broadening the potential applications of metal valves in drug delivery systems. The drug storage chamber, coupled with the sponge adsorption method, allows the system to carry and deliver multiple types of drugs. The flexibility and network structure of the DTME system enable it to conform to complex tissue morphologies, support normal tissue growth, and minimize mechanical damage to the tissue. By utilizing biodegradable materials as primary components of the system, we eliminate the need for secondary surgical removal, thereby preventing further injury to the patient.

RESULTS

Device design and fabrication

The system consisted of a biodegradable flexible network electrode integrated with drug delivery and signal monitoring functions, coupled with an electrophysiological device (Figure 1B). This multifunctional flexible electrode could partially activate the Mg valve through electrical stimulation, thereby triggering drug release. As the valve naturally corroded in a moist environment or underwent accelerated corrosion through electrical stimulation, leading to the full exposure and expansion of the P-sponge, the electrode could continue to function as a recording electrode. The signals collected by the recording electrode were analyzed by the electrophysiological device to guide subsequent treatment

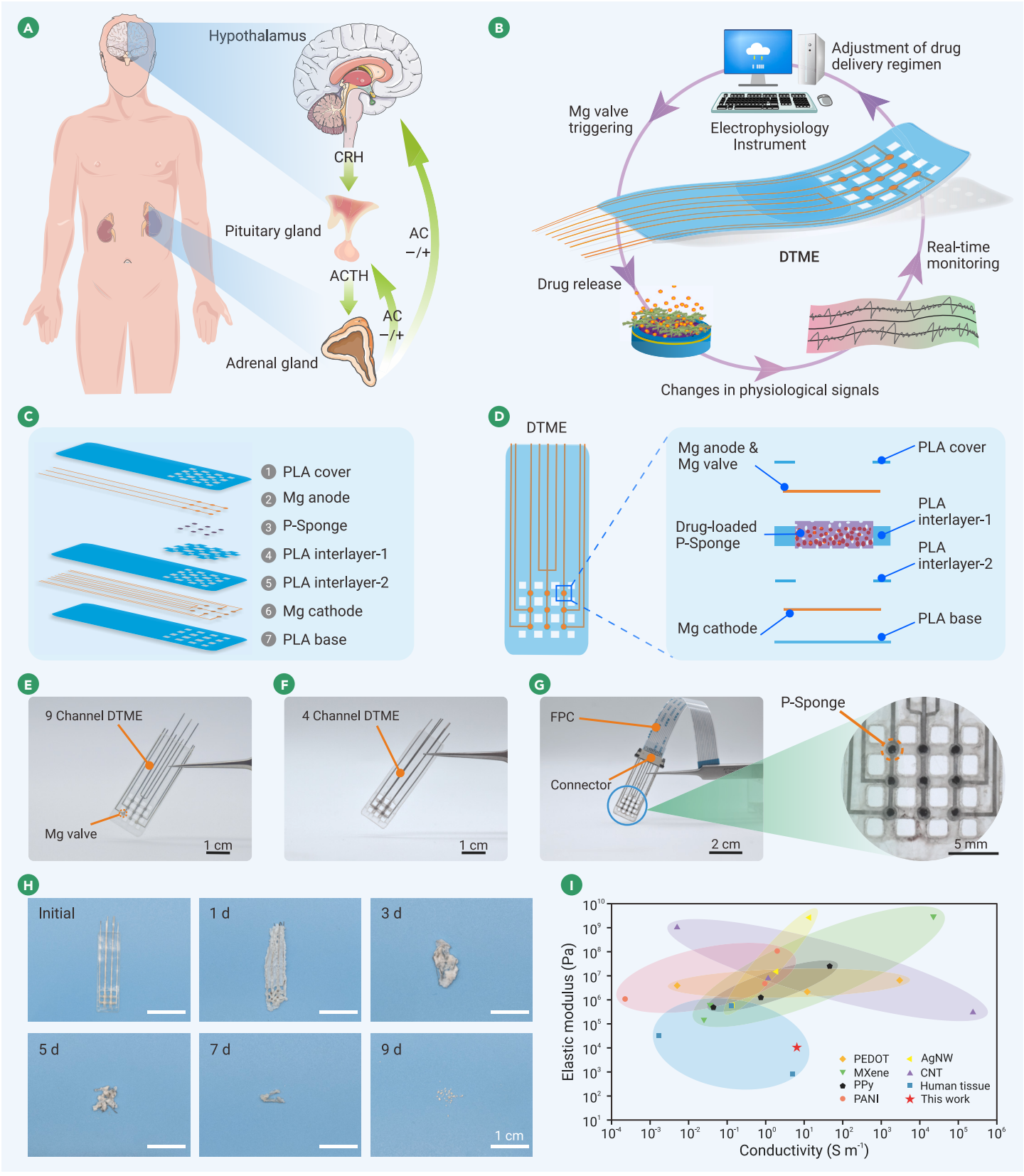

Figure 1. Overview of the multichannel DTME (A) Schematic of the hypothalamic-pituitary-adrenal axis (HPA axis) feedback regulation system. (B) The working principle of DTME, illustrating the biomimetic human feedback regulation mechanism. (C) Exploded view of the structure of 9-channel DTME. (D) Cross-sectional view of the drug-carrying chamber and electrode site within the DTME. (E) Image of the 9-channel DTME configuration. (F) Image of the 4-channel DTME configuration. (G) Photograph displaying all valves in the open position for the 9-channel DTME. (H) Accelerated dissolution of the entire DTME system. (I) Quantification of the elastic modulus and the conductivity of various tissues and conductive composites. The P-sponge developed in this study is marked with a red star, and values for other conductive composites from the literature are also shown, with detailed data provided in Table S1.

decisions. Flexibility and degradability are essential characteristics for implantable flexible electrodes.[46-48] To address these needs, PLAs were prepared and processed into components such as the PLA cover, PLA interlayer-1, PLA interlayer-2, and PLA base, which served as encapsulation material for the DTME (Figure 1C). The customized Mg foil leads were arranged as the cathode (bottom) and anode (top) within the system (Figure 1D). The P-sponges were strategically placed in the PLA drug-carrying compartments between the cathode and anode electrodes. These sponges acted as carriers for the drug solution and provided the water to facilitate the slight corrosion and partial opening of the valve under electrical stimulation and a conductive circuit for subsequent complete valve opening in wet or liquid environments. Our modular design approach allowed for individual customization and enabled the rapid fabrication of various DTMEs tailored to specific requirements (Figures 1E and 1F). The structural design allowed for a complete opening of all channels to expose the P-sponge (Figure 1G).

PLA, the primary material used in the DTME, demonstrated excellent flexibility (Figures S1A and S1B). To further evaluate the flexibility of the DTME, repeated bending tests were conducted (Figure S1C). The results indicated that the DTME, encapsulated with multiple layers of PLA, retained its flexibility even after extensive testing. Over the course of 1,000 bending cycles, the load on the DTME remained stable and significantly lower than that of the polyethylene glycol terephthalate (PET) (Figures S1D–S1F). Additionally, the excellent conformity of the DTME to the viscoelastic hydrogel further underscored its superior flexibility (Figure S2). Biodegradability is a critical characteristic for *in vivo* implants. Our results indicate that Mg foils corroded gradually over time in a PBS environment at 37°C (Figure S3). Although, in theory, the Mg foil valve can remain intact for several days (Figure S4), its actual functional duration is further shortened due to the complex physiological environment and galvanic corrosion. Despite PLA exhibiting slight corrosion, its inherent properties result in a slower degradation under these conditions. The P-sponge also showed no significant signs of degradation (Figure S3). Despite the P-sponge playing an essential role in drug delivery and sensing, its relatively small proportion within the device minimizes its impact on the overall degradation of the device. To further assess the biodegradability of the device, accelerated degradation experiments were conducted at a higher temperature. The results confirmed that the main body of the device can be completely degraded, thus meeting the requirements for biological absorption (Figure 1H). Compared to existing research, our study demonstrated that the P-sponge, when in contact with tissues, maintained good electrical conductivity and an elastic modulus similar to that of human tissues. This allows for active control of drug release while providing stable monitoring of electrophysiological signals without causing mechanical damage to the surrounding tissues (Figure 1I).

Properties of the P-sponge and the valve-triggering mechanism

Conductive hydrogels have garnered significant attention for their favorable mechanical, electrical, and biocompatible properties, making them suitable for a wide range of applications.[49,50] However, in the DTME system discussed here, conventional hydrogels were inadequate for the demands of rapid diagnosis and treatment. To overcome this limitation, a novel electrode material known as P-sponge, derived from P-hydrogel (P-gel), was developed to function as multifunctional electrodes (Figures 2A and S5).[49,51] Compared to P-gel, P-sponge had a lower modulus of elasticity (Figure 2B), enhancing its suitability for use as bioelectrodes. It also demonstrated excellent resilience, with the ability to return to its original shape and maintain structural stability even under applied pressure (Figure S6; Video S1). The P-sponge also exhibited superior conductivity (Figures 2C and S7) and lower electrochemical impedance (Figures 2D and 2E). These properties enabled P-sponges to achieve excellent signal acquisition capabilities, comparable to those of commercial electrodes (Figure S8). Furthermore, while the drug release rate from P-gel was not significantly affected by electrical stimulation, the P-sponge showed a markedly enhanced drug release rate under electrical stimulation (Figures S9 and S10). Although neither the P-sponge nor the P-gel is electrically contractile, the gas generated by the free water in the P-sponge in response to electrical stimulation accelerates the drug release rate. In contrast, achieving such acceleration with the bound water within P-gel is challenging. Given the excellent performance of P-sponge in terms of conductivity, mechanical properties, and drug delivery, it was selected as the preferred electrode material for simultaneous drug delivery and signal acquisition in the DTME system.

The electrodes were primarily encapsulated by seven accessories, with the anodic Mg valve, the cathodic Mg electrode, and the drug-containing P-sponge sandwich serving as the key elements involved in both treatment and diagnosis (Figure 2F). Despite the fact that maintaining a thin DTME layer only mildly triggered the formation of corrosion holes in the valve, which was insufficient to fully open the valve and expose the P-sponge, it could still lead to drug leakage. When the thickness of the drug-loaded pores and the chamber volume were increased to allow the P-sponge to provide sufficient water, electrical stimulation could induce more severe corrosion from the inside out, leading to more significant valve degradation and opening (Figure 2G; Video S2). Thanks to its excellent elastic recovery, the P-sponge rehydrated and swelled upon contact with tissue in a humid environment, simultaneously releasing the drug into the tissue and enabling real-time monitoring (Figure S11; Video S3). To further explore the valve's opening behavior, voltage changes were monitored. It was observed that with a constant valve thickness and diameter, increased constant currents resulted in an earlier appearance of the voltage threshold (Figure 2H).[52] Additionally, a direct relationship was found between the valve thickness and appearance time of the voltage threshold at a fixed diameter and current, consistent with Faraday's law (Figure 2I).[52,53] Moreover, valves with smaller orifice diameters corroded more quickly when the thickness and current were held constant (Figure 2J). Although the presence of a plateau phase in the voltage readings did not indicate the complete opening of the valve due to the safety threshold limitations of the equipment, it did demonstrate how various factors influenced the valve's opening behavior. Figure S12 illustrates the release of rhodamine from a single-channel DTME and the drug release profile of bovine serum albumin (BSA) from a single-channel DTME, highlighting the system's drug delivery capability. The control capabilities of a 4-channel DTME were assessed by sequentially activating different channels through electrical stimulation and monitoring the resultant drug release profiles. The results demonstrated that drug release occurred rapidly following valve opening in a moist or liquid environment. As electrical stimulation sequentially triggered other valves, the cumulative percentage of drug release in the solution increased stepwise (Figure 2K). Although the drug release profile did not exhibit a perfectly uniform increase, it was sufficient to demonstrate that the DTME could exert some control over multiple channels. This ability to control drug release, even when the DTME was bent, highlights its adaptability to complex physiological environments, suggesting its potential for therapeutic applications (Figure S13).

Cell growth behavior under DTME regulation

DTMEs were cocultured with HeLa and human umbilical vein endothelial cells (HUVECs) to assess the drug delivery capability of the DTME (Figures 3A and 3B). Optical and fluorescence images, with phalloidin staining for cell F-actin (red) and 4′,6-diamidino-2-phenylindole (DAPI) staining for the cell nucleus (blue), were captured before and after valve activation (Figures 3C and 3E). DTMEs loaded with paclitaxel (PTX) and vascular endothelial growth factor (VEGF) were placed in the culture dishes containing HeLa cells and HUVECs for 1 h, respectively. As shown in Figures 3C (coculture-1 h) and 3E (coculture-1 h), both HeLa cells and HUVECs exhibited no significant morphological changes after 1 h of coculture. The viability of HeLa cells and HUVECs also remained stable, with no significant differences observed in cell activity following the 1-h coculture with the DTME (Figures 3D and 3F). However, after triggering the valve and incubating for an additional 2 h, a reduction in the activity of HeLa cells was observed, indicating that the release of PTX inhibited the proliferation of HeLa cells (Figure 3C, drug release-2 h). This decrease in HeLa cell activity was further confirmed by both optical and fluorescence imaging (Figure 3D). In contrast, in the incubation experiments with HUVECs, the materials did not adversely affect cell viability. When the valve was opened for 2 h, HUVECs showed an increase in cell activity due to the release of VEGF (Figure 3E, drug release-2 h). The results from the Cell Counting Kit-8 (CCK-8) assay were consistent with the trends observed in the images (Figure 3F).

DTME for signal acquisition and electrical stimulation

The functionality of DTMEs as physiological signal electrodes was validated in rats using DTMEs with an exposed P-sponge (Figure S14). 4-Channel DTMEs were implanted subcutaneously in the anesthetized rats, and ECG signals were recorded. All 4-channel DTMEs operated effectively, successfully acquiring ECG signals from the rats (Figure 4A). Further analysis of individual ECG signal

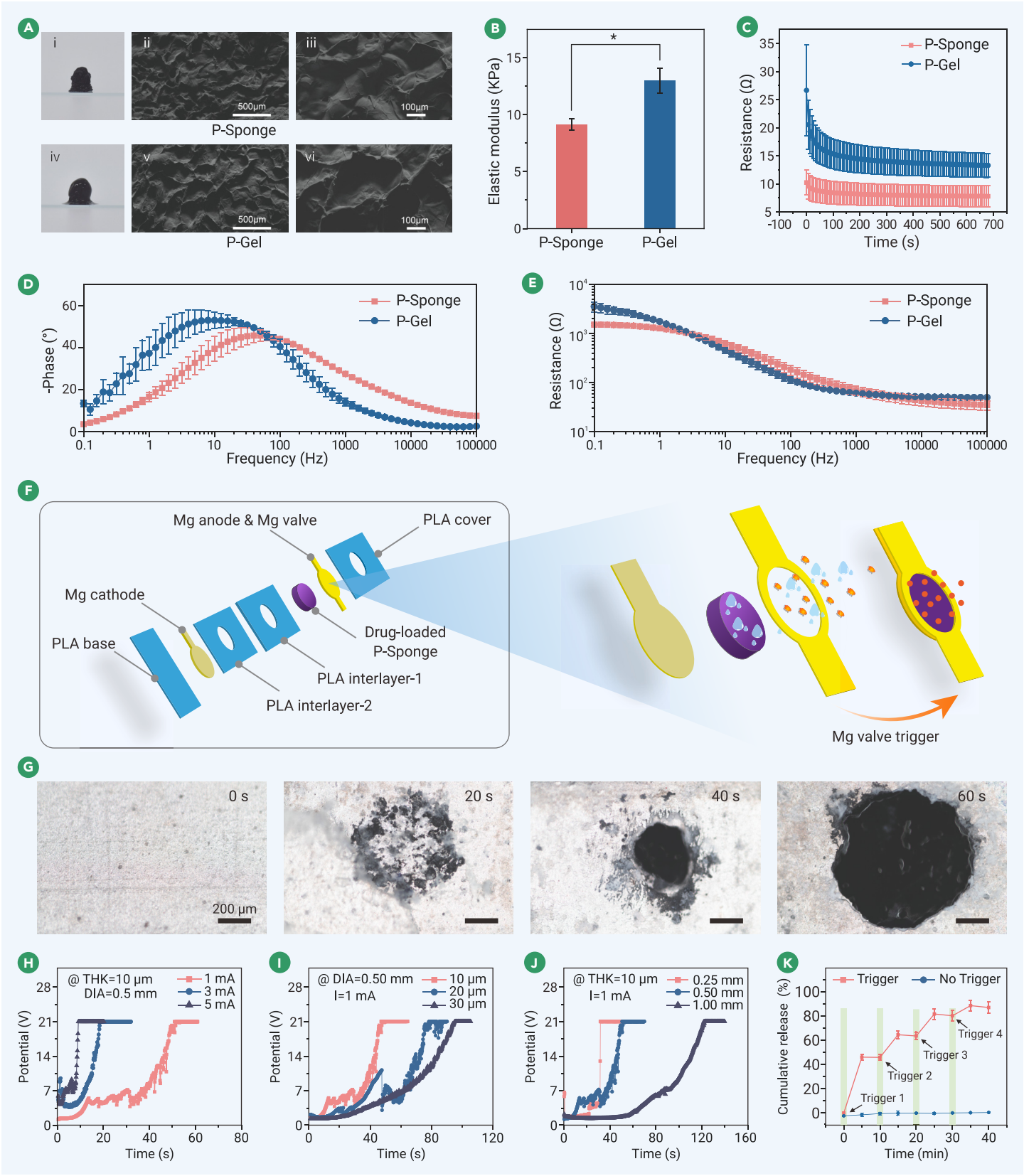

Figure 2. Materials properties and work mechanism of DTME (A) Microstructure comparison between P-sponge and P-gel. (B) Comparison of elastic modulus between P-sponge and P-gel. (C) Resistance of P-sponge and P-gel. (D) Electrical impedance spectroscopy of P-sponge and P-gel, displaying the impedance phase over a frequency sweep from 1 MHz to 0.1 Hz (n = 3). (E) Electrical impedance spectroscopy of P-sponge and P-gel measured, displaying the impedance modulus over a frequency sweep from 1 MHz to 0.1 Hz (n = 3). (F) Exploded view of the DTME charge chamber structure and the mechanism for opening the Mg valve. (G) Sequential images showing the electrochemical etching of the Mg valve, with repeated cleaning of the electrode surface with chromic acid followed by water. (H) Dependence of the trigger time on applied current at fixed Mg valve size. (I) Influence of Mg valve thickness on trigger time at a constant current and valve diameter. (J) Effect of Mg valve diameter on trigger time at a fixed current and valve thickness. (K) Pulsed drug release from a 4-channel DTME, showing the cumulative release profile (n = 4). Bars are mean ± SD (B, C, D, E, and K). ns, not significant; *p < 0.05, **p < 0.01, ***p < 0.001; one-way ANOVA adjusted by Tukey's test.

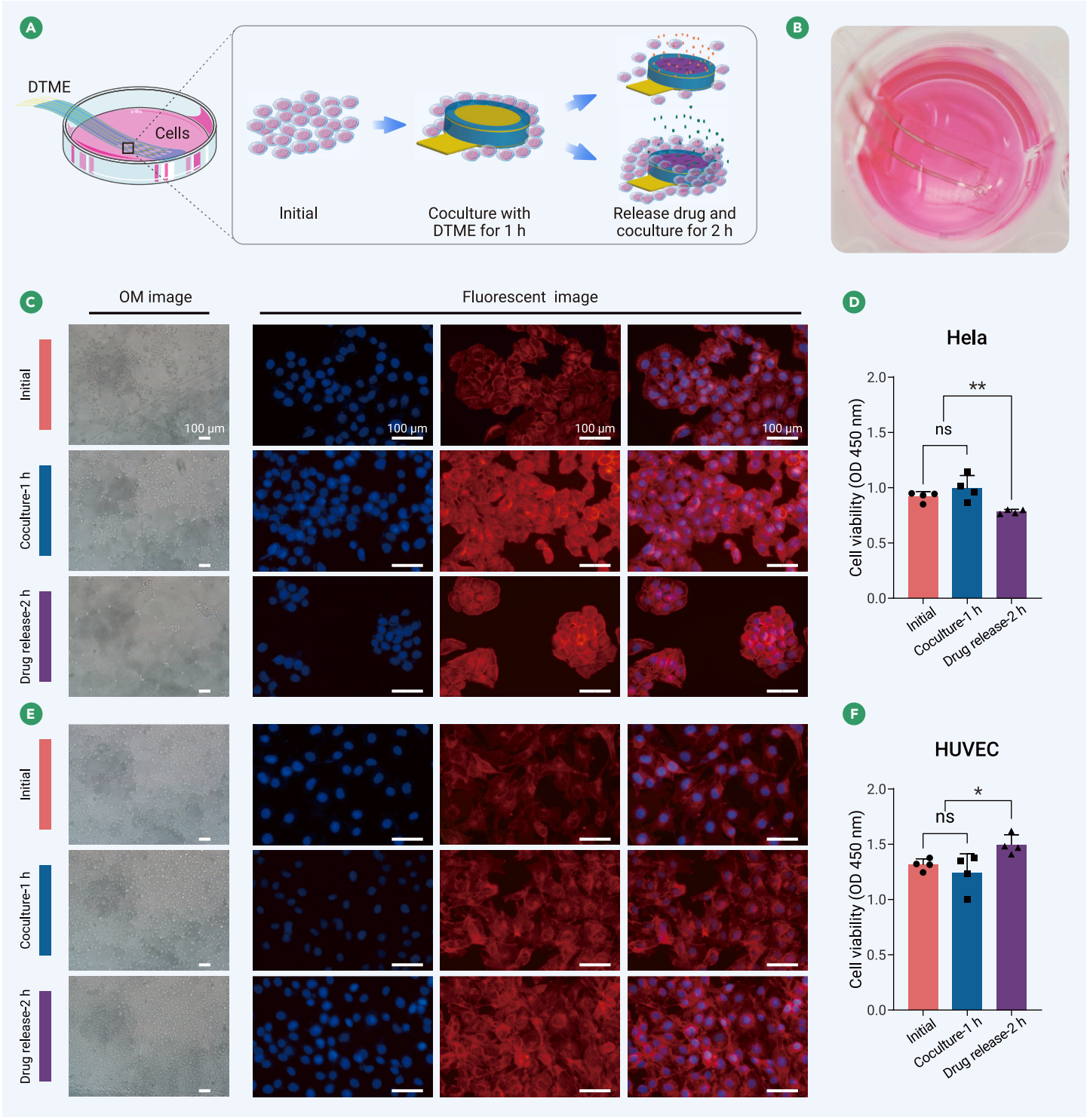

Figure 3. DTME regulated cell activity *in vitro* through drug release (A) Schematic illustration of the experimental setup showing the effect of drug release from DTME on cells. (B) Photographs of DTME cocultured with cells. (C) Optical microscopy (left) and fluorescence microscopy (middle) images of HeLa cells stained with phalloidin (red, F-actin) and DAPI (blue, nuclei) before and after drug release from the DTME. (D) Comparison of HeLa cells viability before and after PTX release from electrodes as measured by CCK-8 assay (optical density [OD] 450 nm). (E) Optical microscopy (left) and fluorescence microscopy (middle) images of HUVECs stained with phalloidin (red, F-actin) and DAPI (blue, nuclei) before and after drug release from the DTME. (F) Comparison of HUVECs' cell viability before and after VEGF release from the electrodes as measured by CCK-8 assay (OD 450 nm). Bars are mean ± SD (D, F). ns, not significant; *$p < 0.05$, **$p < 0.01$, ***$p < 0.001$; one-way ANOVA adjusted by Tukey's test.

waveforms revealed a high degree of consistency across the four channels, with each displaying typical characteristics of the P, Q, R, S, and T segments of the ECG waveform. To further verify the applicability of the 4-channel DTMEs, open-chest surgery was performed on anesthetized rats, and the DTMEs were placed on the heart's surface for ECG signal acquisition (Figure 4B). The results showed that the ECG waveforms from channels 1, 2, and 4 were consistent and exhibited uniform frequencies. However, the ECG signals from channel 3 showed irregular and intermittent waveforms. Despite the lower heart rate and abnormal waveforms caused by the adverse effects of deep anesthesia and surgery, the ECG waveform was more pronounced due to the direct contact with the heart. However, the variability in data collected from different channels, particularly the instability observed in channel 3, highlighted a challenge with the adhesion properties of the encapsulating materials, including P-sponge. This limitation hindered the DTMEs' ability to maintain consistent adherence to the dynamic surface of the beating heart, leading to signal acquisition instability. These findings underscore the need to enhance the adhesion properties of DTMEs to ensure

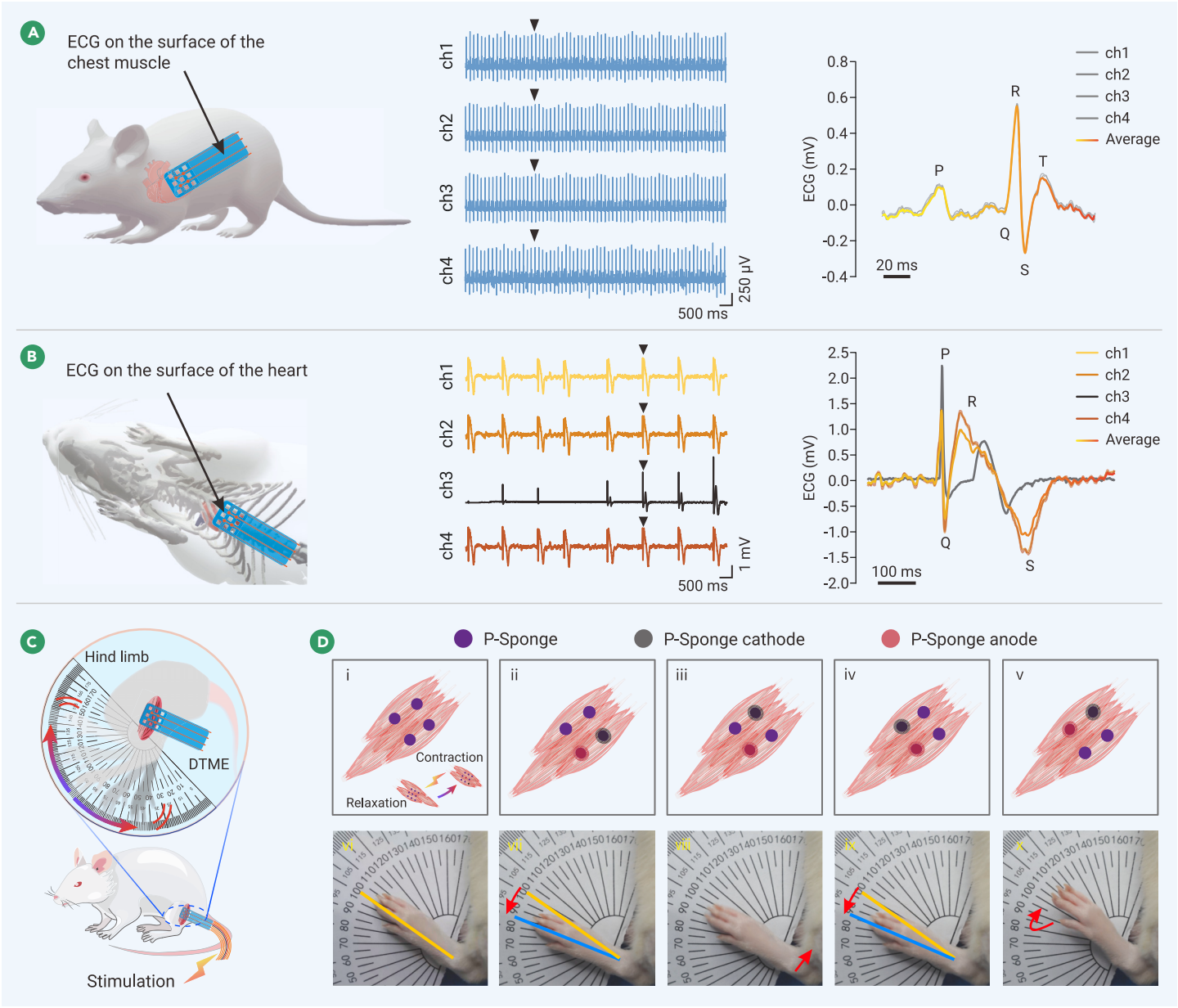

Figure 4. Functional validation of the DTME as a recording and stimulating electrode (A) Schematic illustration of a multichannel electrode measuring ECG signals subcutaneously in rats (left). The middle image shows ECG signals recorded from a 4-channel electrode, and the right image presents the simultaneous fitting and averaging of multiple single waveforms. (B) Schematic illustration of direct ECG signals measurement on the rat heart surface using DTME (left). The middle image shows ECG signals accurately recorded by the 4-channel DTME on the rat heart surface, while the right image presents the simultaneous fitting and averaging of multiple channel waveforms. The figure was created thanks to the rat skeleton three-dimensional (3D) model shared by Doney et al. (https://3dprint.nih.gov/license/cc).[54] (C) Schematic illustration of rat anterior tibial muscle contraction under electrical stimulation. (D) Photographs from Video S4 showing DTME stimulation of exposed muscles in the hind limbs of rats. The images depict various responses: major oscillations (vii), muscle contractions (viii), minor oscillations (xi), and up-down oscillations (x), triggered by adjusting the array positioning or changing the electrodes of the stimulation pulse. The top row (i–v) indicates the stimulation site of the electrode, while the bottom row (vi–x) show the maximum limb deflection (activated) during stimulation.

stable and reliable capture of electrophysiological signals *in vivo* under dynamic conditions.

To validate the stimulation function of the DTME, it was placed on the anterior tibialis muscle of the rat's hind leg (Figure 4C). As demonstrated in Figure S15, the DTME successfully functioned as a stimulation electrode, delivering electrical stimulation at varying parameters with a threshold of 5 V. By setting different sites of the four channels as either cathode or anode and targeting various positions of the hindlimb muscles (Figure 4D), a range of responses were elicited. These responses included intense left-right oscillation of the foot, slight left-right oscillation, simple muscle contraction, and up-down oscillation of the foot (Video S4).

In vivo multifunctionality studies of DTME

To further prove the dual functionality of the DTME, an amplified and thickened dual-channel DTME was placed on the subcutaneous muscular surface of rat's chest (Figure S16A). We simultaneously recorded the ECG of the rats using both commercial electrodes and the exposed P-sponge electrode from channel 1. After establishing a baseline by recording the rats' normal heart rate, we induced arrhythmia using a $CaCl_2$ solution. Upon observing a drop in heart rate intensity, saline was released in the control group, while noradrenaline bitartrate was released in the experimental group. A comparison of heart rate intensity before and after drug release revealed that the heart rate intensity in the control group did not recover after saline release (Figure S16B). In contrast, in the experimental group, the heart rate intensity returned to normal levels after the release of noradrenaline bitartrate (Figure S16C). We also evaluated the DTME's functionality using an epilepsy model (Figure 5A). Brain activity in mice was monitored following the administration of pilocarpine, and the device was used to release a drug upon detection of epileptiform activity. In the control group, the release of saline failed to stop the seizures (Figure 5B). However, in another group, the release of midazolam successfully suppressed the seizures (Figure 5C).

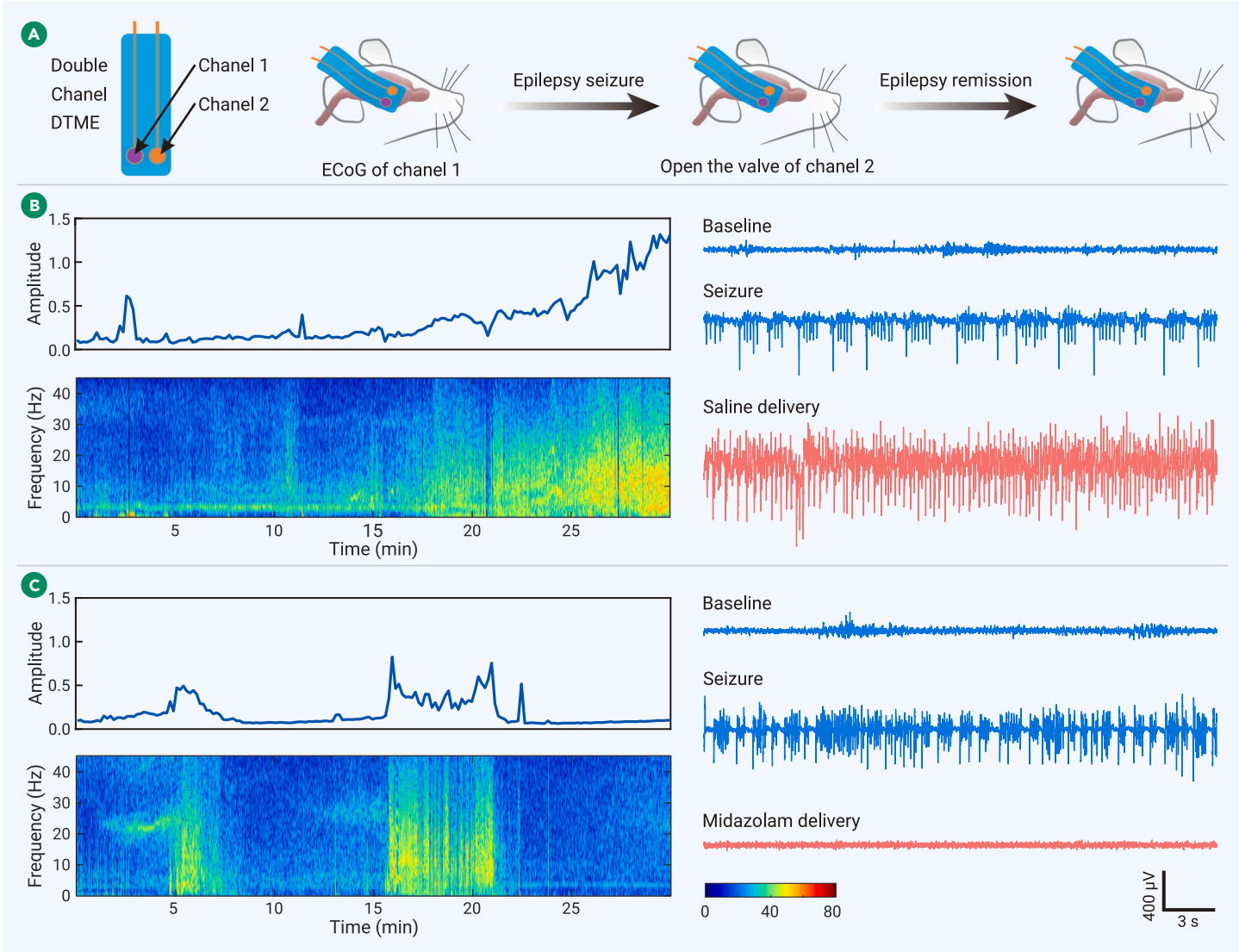

Figure 5. Demonstration of synergistic diagnostic and therapeutic functions (A) Dual-channel DTME monitors epileptic ECoG signaling in the cerebral cortex of mice, triggering the opening of the Mg valve to release drugs. The figure was realized thanks to the rat brain 3D model shared by Pohl et al. (Figshare: https://doi.org/10.6084/m9.figshare.823546.v1). (B) Saline was delivered using DTME after the onset of seizure induction. (C) Midazolam was delivered using DTME after the onset of seizure induction.

Although this type of treatment could not achieve long-term suppression or fully treat disease flare-ups, it demonstrated potential clinical significance as a transitional treatment.

Cytocompatibility and biocompatibility of P-sponge and DTME

The coculture results of the P-sponge with C2C12 cells showed no significant cell death in either the control or P-sponge groups (Figures 6A and 6B). Cell viability of the P-sponge group showed no significant difference compared to the control group. After 72 h of coculture, cell viability in the P-sponge group significantly increased compared to 24 h, indicating the good cytocompatibility of the P-sponge (Figure 6C). A similar experiment was conducted to assess the cytocompatibility of DTMEs. The DTME group exhibited fewer dead cells compared to the control group, with overall cell growth remaining robust (Figures 6D and 6E). Although the DTME group showed slightly lower average cell viability relative to the control group, statistical analysis revealed no significant difference, and cell viability significantly increased after 72 h compared to 24 h (Figure 6F). To evaluate biocompatibility, the P-sponge and multichannel DTME were implanted into rats. Hematoxylin and eosin (H&E) and Masson staining of tissue samples collected 4 weeks post-implantation showed that the tissues surrounding the P-sponge and DTME exhibited no significant inflammatory reactions or fibrosis, similar to the control group (Figure 6G). These findings indicate that the long-term implantation of the DTME and P-sponge in animals did not provoke a strong foreign body reaction. Combined with the results of cellular experiments, it was evident that both the DTME and P-sponge can be safely used as implants in animals for extended periods of time.

DISCUSSION AND CONCLUSION

In this study, we introduced a biodegradable, multifunctional flexible array electrode system designed for integrated diagnostics and therapeutics, combining drug delivery with bioelectrical signal acquisition. The system is primarily constructed from biodegradable PLA and Mg foil, ensuring mechanical compatibility while minimizing potential tissue damage. Unlike conventional drug-carrying coatings or hydrogels, which may pose a risk of drug leakage, our system employs an Mg valve that ensures zero leakage over a period of time by sealing the drug storage chamber. Upon electrical stimulation, the anodic Mg valve rapidly reacts with the stored water in the P-sponge, corroding and opening the valve, leading to drug release. Although the limited water within the P-sponge could only slightly and partly open the valve, natural corrosion facilitated by abundant moisture from the surrounding tissue or environment or accelerated by electrical stimulation could eventually lead to the complete opening of the valve. We also introduced the P-sponge, a material with high electrical conductivity that enhances mechanical compatibility and signal stability while minimizing tissue damage, thereby optimizing diagnostic outcomes. *In vitro* experiments demonstrated the DTME's capability for controlled drug release, while *in vivo* animal studies validated its effectiveness in drug delivery and real-time monitoring. The DTME exhibited integrated diagnostic and therapeutic

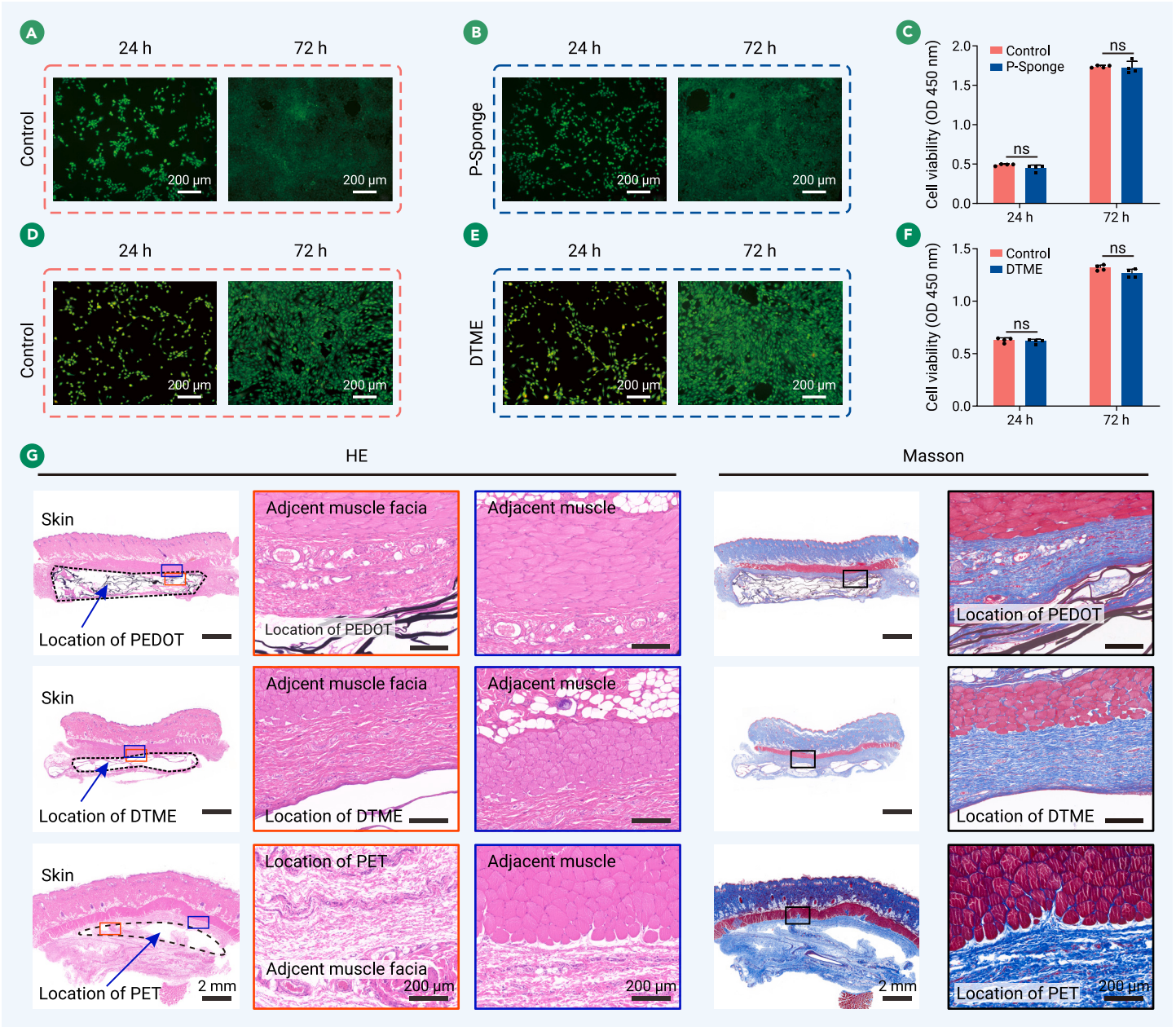

Figure 6. Cytocompatibility and biocompatibility studies (A) Live-dead staining images of cells in the control group. (B) Live-dead staining images of cells cocultured with P-sponge. (C) Comparison of cell viability between the control and P-sponge coculture groups (n = 4). (D) Live-dead staining images of cells in the control group. (E) Live-dead staining images of cells cocultured with DTME. (F) Comparison of cell activity between control and DTME groups after 24 and 72 h (n = 4). (G) H&E (left) and Masson (right) images of stained tissue sections at 4 weeks. Bars are mean ± SD (C, F). ns, not significant; *p < 0.05, **p < 0.01, ***p < 0.001; one-way ANOVA adjusted by Tukey's test.

capabilities, particularly in the management of acute conditions. Both Mg and PLA materials are degradable, and the overall degradation rate of the system can be adjusted by varying the molecular weight of PLA and the thickness of the Mg foil, allowing for control over the system's operational duration and degradation cycle. The modular design supports personalized customization, enabling DTMEs be tailored to specific clinical needs by adjusting channels, electrode sizes, and drug types. This system offers several advantages, including a simplified structural design, cost-effective fabrication, and compatibility with mainstream physiological devices, making it accessible even in resource-limited settings.

Although the system integrated both drug delivery and signal acquisition functions, the use of biodegradable materials posed challenges to the *in vivo* stability of DTME, limiting its suitability for long-term implantation. The higher potential of materials like PEDOT, conductive adhesive, and the connecting wires further diminishes the control capacity of the valve and the recording capability of the electrodes in practical long-term applications. Therefore, finding the optimal balance between degradability and performance stability is crucial for implantable flexible electrodes. To mitigate these issues, using a more stable metal like gold foil in place of Mg or applying surface treatment techniques to enhance the corrosion resistance and conductivity of Mg could be an effective strategy. Additionally, employing encapsulation materials with longer degradation cycles, more stable biodegradable conductive polymers, and electrically responsive sponges capable of multiple administrations can enhance the feedback modulation capabilities of DTMEs. Moreover, while the convergence of drug delivery and signal acquisition functions at the same site enhances integration, it compromises the precision of each function. Although the complete triggering of the valve and drug release can be independently achieved by adjusting the diameter and thickness of the drug-loaded pores, under conditions that also ensure good flexibility, the system can only slightly trigger the valve and drug release. Complete valve activation and drug release still depend on moisture provided by the external environment. Consequently, enhancing the structure of drug-loading sites is imperative to improve the flexibility and drug delivery capability of DTMEs. The series-connected valves, designed to reduce the number of control wires, have compromised the system's control precision. Therefore, optimizing the electrode array

design is essential to addressing the challenges of valve series connection and mitigating cross-talk between recording electrodes. The lack of adhesion not only reduces the system's ability to collect signals from moving tissue surfaces but also increases the difficulty of securing to static tissue. Developing degradable adhesive encapsulation materials and electrodes could enhance its applicability. While electrophysiological signals can be used to assess disease progression, their variability due to individual differences and various influencing factors can complicate interpretation. Therefore, establishing a standardized evaluation system is essential for accurately determining the severity of disease onset and the extent of recovery.

Moreover, expanding the capabilities of the P-sponge to include sensing functions for pH, temperature, glucose, and other signals within the DTI device would enable a more comprehensive approach to diagnosis and treatment, addressing complex clinical needs. DTME devices hold significant promise as tools for telemedicine, supporting physicians in remote patient monitoring and enabling timely interventions, thus offering a novel avenue for disease management. Furthermore, integrating DTMEs with wireless-powered devices and chips would enable closed-loop processing capabilities, facilitating real-time disease monitoring and personalized treatment without continuous intervention from physicians and patients.

MATERIALS AND METHODS

See the supplemental information for details.

REFERENCES

1. Tan, M., Xu, Y., Gao, Z., et al. (2022). Recent advances in intelligent wearable medical devices integrating biosensing and drug delivery. Adv. Mater. ***34***: e2108491. https://doi.org/10.1002/adma.202108491.
2. Li, P., Lee, G.H., Kim, S.Y., et al. (2021). From diagnosis to treatment: recent advances in patient-friendly biosensors and implantable devices. ACS Nano ***15***: 1960–2004. https://doi.org/10.1021/acsnano.0c06688.
3. Zhang, Y., Li, D., Liu, Y., et al. (2023). 3D-bioprinted anisotropic bicellular living hydrogels boost osteochondral regeneration via reconstruction of cartilage-bone interface. Innovation ***5***(1): 100542. https://doi.org/10.1016/j.xinn.2023.100542.
4. Ning, T., Yang, F., Chen, D., et al. (2022). Synergistically detachable microneedle dressing for programmed treatment of chronic wounds. Adv. Healthcare Mater. ***11***: 2102180. https://doi.org/10.1002/adhm.202102180.
5. Dall, T.M., Gallo, P.D., Chakrabarti, R., et al. (2013). An aging population and growing disease burden will require alarge and specialized health care workforce by 2025. Health Aff. ***32***: 2013–2020. https://doi.org/10.1377/hlthaff.2013.0714.
6. Wang, D., Zhang, J., Liu, Q., et al. (2020). 3D printing challenges in enabling rapid response to public health emergencies. Innovation ***1***(3): 100056. https://doi.org/10.1016/j.xinn.2020.100056.
7. Yang, F., Xu, C., Zhang, W., et al. (2023). Biodegradable magnesium incorporated microspheres enable immunomodulation and spatiotemporal drug release for the treatment of osteonecrosis of the femoral head. Compos. B. Eng. ***250***: 110430. https://doi.org/10.1016/j.compositesb.2022.110430.
8. Sharma, H.B., Vanapalli, K.R., Cheela, V.S., et al. (2020). Challenges, opportunities, and innovations for effective solid waste management during and post COVID-19 pandemic. Resour. Conserv. Recycl. ***162***: 105052. https://doi.org/10.1016/j.resconrec.2020.105052.
9. Li, Z., Ruan, C., and Niu, X. (2023). Collagen-based bioinks for regenerative medicine: Fabrication, application and prospective. Med. Nov. Technol. Dev. ***17***: 100211. https://doi.org/10.1016/j.medntd.2023.100211.
10. Nguyen, T., Duong Bang, D., and Wolff, A. (2020). 2019 novel coronavirus disease (COVID-19): paving the road for rapid detection and point-of-care diagnostics. Micromachines (Basel) ***11***: 306. https://doi.org/10.3390/mi11030306.
11. Jiang, S., Zhang, T., Zhou, Y., et al. (2023). Wearable ultrasound bioelectronics for healthcare monitoring. Innovation ***4***(4): 100447. https://doi.org/10.1016/j.xinn.2023.100447.
12. Boutry, C.M., Beker, L., Kaizawa, Y., et al. (2019). Biodegradable and flexible arterial-pulse sensor for the wireless monitoring of blood flow. Nat. Biomed. Eng. ***3***: 47–57. https://doi.org/10.1038/s41551-018-0336-5.
13. Zhang, T., Liu, N., Xu, J., et al. (2023). Flexible electronics for cardiovascular healthcare monitoring. Innovation ***4***(4): 100485. https://doi.org/10.1016/j.xinn.2023.100485.
14. Xia, X., Liang, Q., Sun, X., et al. (2022). Intrinsically electron conductive, antibacterial, and anti-swelling hydrogels as implantable sensors for bioelectronics. Adv. Funct. Mater. ***32***: 2208024. https://doi.org/10.1002/adfm.202208024.
15. Wang, H., Ding, Q., Luo, Y., et al. (2024). High-performance hydrogel sensors enabled multimodal and accurate human-machine interaction system for active rehabilitation. Adv. Mater. ***36***: 2309868. https://doi.org/10.1002/adma.202309868.
16. Tringides, C.M., Vachicouras, N., de Lazaro, I., et al. (2021). Viscoelastic surface electrode arrays to interface with viscoelastic tissues. Nat. Nanotechnol. ***16***: 1019–1029. https://doi.org/10.1038/s41565-021-00926-z.
17. Xu, L., Gutbrod, S.R., Bonifas, A.P., et al. (2014). 3D multifunctional integumentary membranes for spatiotemporal cardiac measurements and stimulation across the entire epicardium. Nat. Commun. ***5***: 1–10. https://doi.org/10.1038/ncomms4329.
18. Afanasenkau, D., Kalinina, D., Lyakhovetskii, V., et al. (2020). Rapid prototyping of soft bioelectronic implants for use as neuromuscular interfaces. Nat. Biomed. Eng. ***4***: 1010–1022. https://doi.org/10.1038/s41551-020-00615-7.
19. Jeong, U.J., Lee, J., Chou, N., et al. (2021). A minimally invasive flexible electrode array for simultaneous recording of ECoG signals from multiple brain regions. Lab Chip ***21***: 2383–2397. https://doi.org/10.1039/d1lc00117e.
20. Tybrandt, K., Khodagholy, D., Dielacher, B., et al. (2018). High-density stretchable electrode grids for chronic neural recording. Adv. Mater. ***30***: 1706520. https://doi.org/10.1002/adma.201706520.
21. Ouyang, J. (2021). Application of intrinsically conducting polymers in flexible electronics. SmartMat ***2***: 263–285. https://doi.org/10.1002/smm2.1059.
22. Shur, M., Fallegger, F., Pirondini, E., et al. (2020). Soft printable electrode coating for neural interfaces. ACS Appl. Bio. Mater. ***3***: 4388–4397. https://doi.org/10.1021/acsabm.0c00401.
23. Kang, Y., Zhang, H., Chen, L., et al. (2022). The marriage of Xenes and hydrogels: fundamentals, applications, and outlook. Innovation ***3***(6): 100327. https://doi.org/10.1016/j.xinn.2022.100327.
24. Li, J., Ding, Q., Wang, H., et al. (2023). Engineering smart composite hydrogels for wearable disease monitoring. Nano-Micro Lett. ***15***: 105. https://doi.org/10.1007/s40820-023-01079-5.
25. Wang, W., Yao, D., Wang, H., et al. (2024). A breathable, stretchable, and self-calibrated multimodal electronic skin based on hydrogel microstructures for wireless wearables. Adv. Funct. Mater. ***34***: 2316339. https://doi.org/10.1002/adfm.202316339.
26. Qazi, R., Gomez, A.M., Castro, D.C., et al. (2019). Wireless optofluidic brain probes for chronic neuropharmacology and photostimulation. Nat. Biomed. Eng. ***3***: 655–669. https://doi.org/10.1038/s41551-019-0432-1.
27. Choi, Y.S., Jeong, H., Yin, R.T., et al. (2022). A transient, closed-loop network of wireless, body-integrated devices for autonomous electrotherapy. Science ***376***: 1006–1012. https://doi.org/10.1126/science.abm1703.
28. Chen, J.C., Kan, P., Yu, Z., et al. (2022). A wireless millimetric magnetoelectric implant for the endovascular stimulation of peripheral nerves. Nat. Biomed. Eng. ***6***: 706–716. https://doi.org/10.1038/s41551-022-00873-7.
29. Silverå Ejneby, M., Jakešová, M., Ferrero, J.J., et al. (2022). Chronic electrical stimulation of peripheral nerves via deep-red light transduced by an implanted organic photocapacitor. Nat. Biomed. Eng. ***6***: 741–753. https://doi.org/10.1038/s41551-021-00817-7.
30. Zhang, Y., Mickle, A.D., Gutruf, P., et al. (2019). Battery-free, fully implantable optofluidic cuff system for wireless optogenetic and pharmacological neuromodulation of peripheral nerves. Sci. Adv. ***5***: eaaw5296. https://doi.org/10.1126/sciadv.aaw5296.
31. Joo, H., Lee, Y., Kim, J., et al. (2021). Soft implantable drug delivery device integrated wirelessly with wearable devices to treat fatal seizures. Sci. Adv. ***7***: eabd4639. https://doi.org/10.1126/sciadv.abd4639.
32. Minev, I.R., Musienko, P., Hirsch, A., et al. (2015). Electronic dura mater for long-term multimodal neural interfaces. Science ***347***: 159–163. https://doi.org/10.1126/science.1260318.
33. Feiner, R., Engel, L., Fleischer, S., et al. (2016). Engineered hybrid cardiac patches with multifunctional electronics for online monitoring and regulation of tissue function. Nat. Mater. ***15***: 679–685. https://doi.org/10.1038/nmat4590.
34. Pang, Q., Lou, D., Li, S., et al. (2020). Smart flexible electronics-integrated wound dressing for real-time monitoring and on-demand treatment of infected wounds. Adv. Sci. ***7***: 1902673. https://doi.org/10.1002/advs.201902673.
35. Jiang, Y., Trotsyuk, A.A., Niu, S., et al. (2023). Wireless, closed-loop, smart bandage with integrated sensors and stimulators for advanced wound care and accelerated healing. Nat. Biotechnol. ***41***: 652–662. https://doi.org/10.1038/s41587-022-01528-3.
36. Xu, G., Lu, Y., Cheng, C., et al. (2021). Battery-free and wireless smart wound dressing for wound infection monitoring and electrically controlled on-demand drug delivery. Adv. Funct. Mater. ***31***: 2100852. https://doi.org/10.1002/adfm.202100852.
37. Rezapour Sarabi, M., Nakhjavani, S.A., and Tasoglu, S. (2022). 3D-printed microneedles for point-of-care biosensing applications. Micromachines (Basel) ***13***: 1099. https://doi.org/10.3390/mi13071099.
38. Mirani, B., Pagan, E., Currie, B., et al. (2017). An advanced multifunctional hydrogel-based dressing for wound monitoring and drug delivery. Adv. Healthcare Mater. ***6***: 1700718. https://doi.org/10.1002/adhm.201700718.
39. Lee, H., Song, C., Hong, Y.S., et al. (2017). Wearable/disposable sweat-based glucose monitoring device with multistage transdermal drug delivery module. Sci. Adv. ***3***: e1601314. https://doi.org/10.1126/sciadv.1601314.
40. Lin, S., Yuk, H., Zhang, T., et al. (2016). Stretchable hydrogel electronics and devices. Adv. Mater. ***28***: 4497–4505. https://doi.org/10.1002/adma.201504152.
41. Kim, B., Seong, K.-Y., You, I., et al. (2018). Touch-actuated transdermal delivery patch for quantitative skin permeation control. Sensor. Actuator. B Chem. ***256***: 18–26. https://doi.org/10.1016/j.snb.2017.10.059.
42. Yin, M., Xiao, L., Liu, Q., et al. (2019). 3D printed microheater sensor-integrated, drug-encapsulated microneedle patch system for pain management. Adv. Healthcare Mater. ***8***: 1901170. https://doi.org/10.1002/adhm.201901170.
43. Gogurla, N., Kim, Y., Cho, S., et al. (2021). Multifunctional and ultrathin electronic tattoo for on-skin diagnostic and therapeutic applications. Adv. Mater. ***33***: 2008308. https://doi.org/10.1002/adma.202008308.
44. Mostafalu, P., Tamayol, A., Rahimi, R., et al. (2018). Smart bandage for monitoring and treatment of chronic wounds. Small ***14***: e1703509. https://doi.org/10.1002/smll.201703509.

45. Turnbull, A.V., and Rivier, C. (1995). Regulation of the HPA axis by cytokines. Brain Behav. Immun. ***9***: 253–275. https://doi.org/10.1006/brbi.1995.1026.
46. Li, W., Liu, Q., Zhang, Y., et al. (2020). Biodegradable materials and green processing for green electronics. Adv. Mater. ***32***: 2001591. https://doi.org/10.1002/adma.202001591.
47. Bai, X., Lin, S., Wang, H., et al. (2018). Room-temperature processing of silver submicron fiber mesh for flexible electronics. npj Flex. Electron. ***2***: 1–7. https://doi.org/10.1038/s41528-017-0016-7.
48. Yang, Q., Liu, T.-L., Xue, Y., et al. (2022). Ecoresorbable and bioresorbable microelectromechanical systems. Nat. Electron. ***5***: 526–538. https://doi.org/10.1038/s41928-022-00791-1.
49. Zhang, S., Chen, Y., Liu, H., et al. (2020). Room-temperature-formed PEDOT: PSS hydrogels enable injectable, soft, and healable organic bioelectronics. Adv. Mater. ***32***: 1904752. https://doi.org/10.1002/adma.201904752.
50. Ding, Q., Zhou, Z., Wang, H., et al. (2023). Self-healable, recyclable, ultrastretchable, and high-performance NO2 sensors based on an organohydrogel for room and sub-zero temperature and wireless operation. SmartMat ***4***: e1141. https://doi.org/10.1002/smm2.1141.
51. Chen, G., Rastak, R., Wang, Y., et al. (2019). Strain-and strain-rate-invariant conductance in a stretchable and compressible 3D conducting polymer foam. Matter ***1***: 205–218. https://doi.org/10.1016/j.matt.2019.03.011.
52. Koo, J., Kim, S.B., Choi, Y.S., et al. (2020). Wirelessly controlled, bioresorbable drug delivery device with active valves that exploit electrochemically triggered crevice corrosion. Sci. Adv. ***6***: eabb1093. https://doi.org/10.1126/sciadv.abb1093.
53. Liu, S., Jia, Z., Yang, F., et al. (2023). Flexible transient bioelectronic system enables multifunctional active-controlled drug delivery. Adv. Funct. Mater. ***33***: 2215034. https://doi.org/10.1002/adfm.202215034.
54. Doney, E., Krumdick, L.A., Diener, J.M., et al. (2013). 3D printing of preclinical X-ray computed tomographic data sets. J. Vis. Exp. ***73***: e50250. https://doi.org/10.3791/50250.

ACKNOWLEDGMENTS

The authors would like to acknowledge support from the National Natural Science Foundation of China (nos. 12272032, 82222076, 82074463, and 12332019), the Beijing Natural Science Foundation (no. L234020), and the 111 Project (no. B13003).

AUTHOR CONTRIBUTIONS

X.N. and Y.F. supervised the project. X.N., S.L., and T.N. conceived the original idea and designed all aspects of the experiments about materials. Jinyu Li designed and guided the animal experiments. S.L. and J.C. prepared the samples and performed the experiments. Y.F. and Jiebo Li processed the metal materials needed for the experiments. S.L., T.N., X.N., and Y.F. wrote the paper. All authors commented on the manuscript.

DECLARATION OF INTERESTS

The authors declare no competing interests.

SUPPLEMENTAL INFORMATION

It can be found online at https://doi.org/10.1016/j.xinn.2024.100705.

LEAD CONTACT WEBSITE

https://bme.buaa.edu.cn/teacherInfo.aspx?catID=7&subcatID=35&curID=246
https://bme.buaa.edu.cn/teacherInfo.aspx?catID=7&subcatID=140&curID=420